2007

Turbulent transfer mechanism in sediment-laden flow

Shu-qing Yang
University of Wollongong, shuqing@uow.edu.au

Turbulent transfer mechanism in sediment-laden flow

Abstract

Characteristics of turbulent flows in rivers can be significantly modified because of the presence of sediment particles and secondary currents/nonuniformity. This paper investigates why the measured vertical distributions of velocity deviate from the log law. In contrast to previous research that attributed the deviation to Richardson number only, this study demonstrates that like Reynolds shear stress (−equation image), momentum flux (uv) caused by the nonzero wall-normal velocity v is also responsible for these deviations. Starting from Reynolds equations, this paper shows that the classical log law can be obtained only when v = 0; otherwise the velocity v results in the deviation. On the basis of experimental data available in the literature, this study shows that in an open channel, v is nonzero because of the coexistence of secondary currents and sediment and, subsequently, the Reynolds shear stress and streamwise velocity are affected. Equations for these interactions are obtained and solved numerically. The validity of the proposed model has been verified using experimental data, and good agreement between the predicted and observed profiles has been achieved.

Keywords

laden, flow, sediment, turbulent, mechanism, transfer

Disciplines

Engineering | Science and Technology Studies

Publication Details

Yang, S. (2007). Turbulent transfer mechanism in sediment-laden flow. Journal of Geophysical Research, 112 (F1), 1-14.

Turbulent transfer mechanism in sediment-laden flow

Shu-Qing Yang[1,2]

Received 7 December 2005; accepted 6 September 2006; published 15 February 2007.

[1] Characteristics of turbulent flows in rivers can be significantly modified because of the presence of sediment particles and secondary currents/nonuniformity. This paper investigates why the measured vertical distributions of velocity deviate from the log law. In contrast to previous research that attributed the deviation to Richardson number only, this study demonstrates that like Reynolds shear stress ($-\overline{u'v'}$), momentum flux (uv) caused by the nonzero wall-normal velocity v is also responsible for these deviations. Starting from Reynolds equations, this paper shows that the classical log law can be obtained only when v = 0; otherwise the velocity v results in the deviation. On the basis of experimental data available in the literature, this study shows that in an open channel, v is nonzero because of the coexistence of secondary currents and sediment and, subsequently, the Reynolds shear stress and streamwise velocity are affected. Equations for these interactions are obtained and solved numerically. The validity of the proposed model has been verified using experimental data, and good agreement between the predicted and observed profiles has been achieved.

Citation: Yang, S.-Q. (2007), Turbulent transfer mechanism in sediment-laden flow, *J. Geophys. Res.*, *112*, F01005, doi:10.1029/2005JF000452.

1. Introduction

[2] Sediment-laden flows play an important role in the evolution of riverbeds, estuaries and coasts and are among the most important agents of geomorphic evolution of the Earth's surface. As a consequence, interactions between turbulent flow and sand particle motion in sediment suspensions are of great interest to hydraulic engineers, coastal engineers, geologists and hydrologists, among others.

[3] Turbulence and secondary currents in natural rivers and laboratory flumes are ubiquitous and play an essential role in sediment transport, and in turn suspended particle motion modifies the turbulence, such as Reynolds shear stress and velocity. It is widely reported that because of fluid-particle interactions, the velocity distribution and turbulence characteristics in sediment-laden flows are different from those of particle-free flows. The difference of velocity distributions in flows with or without suspended sediment has stimulated research in many scientific and technical establishments throughout the world, especially during the last decades, e.g., *Vanoni* [1946], *Einstein and Chien* [1955], *Vanoni and Nomicos* [1960], *Elata and Ippen* [1961], and *Yalin* [1977], etc.

[4] However, in spite of the intense activities, there is yet no general consensus on the mechanism causing velocity difference in sediment-laden flows. *Einstein and Chien* [1955] first linked the variation of Karman coefficient in the classical log law with the Richardson number, which reflects the effect of density stratification. However, the experimental results have not always supported their conclusion. For example, *Elata and Ippen* [1961] conducted experiments with neutrally buoyant particles to eliminate the possible effect of density gradient, and the data show that Karman constant is similarly less than the accepted value of 0.4.

[5] *Coleman* [1981, 1986] introduced the wake function to express the deviation of velocity profile from the log law in sediment-laden flows. He reexamined *Einstein and Chien*'s [1955] experimental data, and concluded that the reduction of Karman coefficient κ could be attributed to the inappropriate use of a curve-fitting technique. He revealed that Karman coefficient is independent of sediment concentration if wake function was introduced. An empirical relationship between the wake strength and Richardson's number was established on the basis of his data. Coleman's argument was supported by *Parker and Coleman* [1986] and *Cioffi and Gallerano* [1991]. However, *Kreeselidze and Kutavaia* [1995] and *Lyn* [1988] found that both Karman coefficient and wake strength vary with sediment concentration.

[6] With the advent of accurate nonintrusive measurements, such as laser Doppler anemometer (LDA) and phase Doppler anemometer (PDA), experimental researchers are able to evaluate the Karman constant in sediment-laden flows, and the experiments confirmed that the value of Karman constant decreases with sediment concentration [*Nezu and Azuma*, 2004; *Best et al.*, 1997; *Muste and Patel*, 1997; *Bennett et al.*, 1998].

[7] Therefore it can be concluded that there is no agreement on which theory is correct. With the objective of making progress toward such a theory, this study focuses on

[1]School of Environmental Science and Engineering, South China University of Technology, Wushan, Guangzhou, China.

[2]Formerly at State Key Laboratory of Hydraulic and Mountain River Engineering, Sichuan University, Chengdu China.

0148-0227/07/2005JF000452

the underlying mechanism why the measured velocity deviates from the widely accepted log law. The interactions of sediment, secondary currents/nonuniformity and streamwise velocity will be investigated. The main purposes of this paper are (1) to reexamine Prandtl's mixing length theorem in sediment-laden flows, (2) to assess the magnitude of wall-normal velocity induced by the secondary currents/nonuniformity and sediment settlement, and (3) to develop a model for the prediction simultaneously of velocity and sediment concentration profiles.

2. Governing Equations in Three-Dimensional Sediment-Laden Channel Flows

[8] *Guo and Julien* [2001] analyzed the momentum equations in sediment-laden flows and they concluded that the governing equations for clear water flows are also valid in sediment-laden flows. Hence, for steady, uniform and fully developed turbulent open channel flows with sediment presence, the governing equation for liquid phase can be derived by adding the continuity equation to the momentum equation as follows [*Yang and McCorquodale*, 2004]:

$$\frac{\partial\left(uv-\tau_{xy}/\rho\right)}{\partial y}+\frac{\partial(uw-\tau_{xz}/\rho)}{\partial z}=gS \tag{1}$$

where y is vertical direction and z is lateral direction as shown in Figure 1a; u is streamwise velocity; v and w are vertical and lateral mean velocities in the y and z directions, respectively; g is gravitational acceleration; S is energy slope; $\tau_{xz}=\mu du/dz-\rho\overline{u'w'}$ and $\tau_{xy}=\mu du/dy-\rho\overline{u'v'}$; μ is dynamic viscosity; $-\rho\overline{u'w'}$ and $-\rho\overline{u'v'}$ are the Reynolds shear stress; uv and uw are momentum fluxes caused by mean velocities; ρ is density of fluid.

[9] Similarly, the mass conservation equation can be written in the following form by adding the continuity equation for liquid phase to the continuity equation for solid phase as follows:

$$\frac{\partial\left(Cv+\overline{C'v'}-C\omega\right)}{\partial y}+\frac{\partial\left(Cw+\overline{C'w'}\right)}{\partial z}=0 \tag{2}$$

where C is sediment concentration by volume, C' is fluctuation of sediment concentration, and ω is particle fall velocity.

[10] In the central region of open channel, the magnitude of the second term on the left-hand side (LHS) of equations (1) and (2) is negligible relative to the first term. Thus equation (1) can be simplified into the following form:

$$\frac{\partial\left(uv-\tau_{xy}/\rho\right)}{\partial y}=gS \tag{3}$$

Integration of equation (3) with the boundary conditions: at $y=y_o$, $u=0$, and $\tau_{xy}=\rho u_*^2=$ boundary shear stress yields

$$\mu du/dy-\rho\overline{u'v'}=\rho u_*^2\left(1-\frac{y}{h}\right)+\rho uv \tag{4}$$

where h is water depth. Equation (4) is similar to the momentum equation of clear water in circular pipe flows in which the negligible wall-normal velocity v leads to $uv=0$.

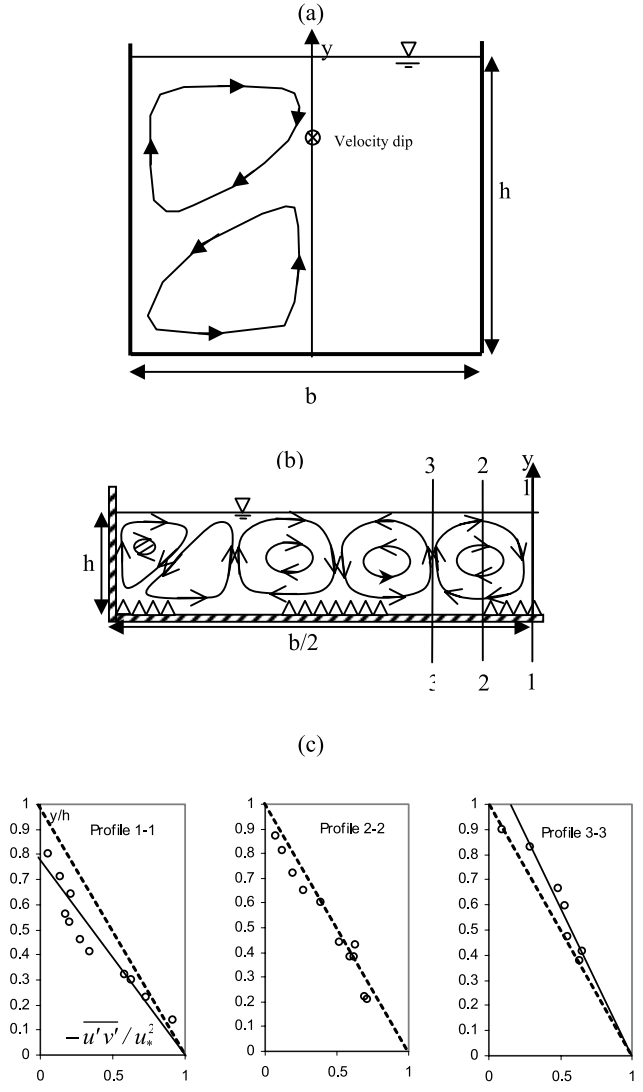

Figure 1. Interaction of wall-normal velocity (or secondary currents), Reynolds shear stress, and dip phenomenon in uniform open channels: (a) A narrow, deep channel from *Nezu* [2002] indicates that along the centerline, the wall-normal velocity v is negative near the free surface but it becomes positive near the bed (the location of maximum velocity is represented by a circled cross). (b) In wide, shallow channels, secondary currents can be generated by bed ridges as observed by *Wang and Cheng* [2005]; (c) y/h versus $-\overline{u'v'}/u_*^2$ measured by *Wang and Cheng* [2005] shows that $-\overline{u'v'}/u_*^2$ is lower, equal to, and higher than the dashed lines where the wall normal velocities are negative, zero, and positive along profiles 1–1, 2–2, and 3–3, respectively.

[11] Equation (4) can be simplified as follows by ignoring the viscous effect

$$-\frac{\overline{u'v'}}{u_*^2}=\left(1-\frac{y}{h}\right)+\frac{uv}{u_*^2} \tag{5}$$

The Reynolds shear stress is often modeled as follows in analogy with the viscous shear stress:

$$\overline{u'v'} = -\varepsilon_f \frac{du}{dy} \tag{6}$$

where ε_f is eddy viscosity of liquid phase.

[12] Similarly, the integration of equation (2) with respect to y yields the following equation:

$$Cv + \overline{C'v'} - C\omega = 0 \tag{7}$$

where the zero mass flux on the free surface is applied to determining the integration constant. The term Cv is conventionally dropped under the assumption of 1-D streamwise flow. The necessity of the additional term Cv in sediment-laden open channel flows has been realized by *Steinour* [1944a, 1944b, 1944c] and *Hawksley* [1951], who noted that sediment presence induces an upward velocity and they suggested that for sediment particles to remain in suspension, the wall-normal velocity v together with the gravitational settlement ω should be balanced by the turbulent diffusion. *Fu et al.* [2005] also stressed the need for the term Cv in equation (7) but they ascribed the vertical velocity v to a fluid-induced lift force.

[13] Turbulent diffusion is commonly expressed by

$$\overline{C'v'} = -\varepsilon_s \frac{dC}{dy} \tag{8}$$

in which ε_s is sediment diffusion coefficient.

[14] In contrast to the widely used equations for sediment-laden flows, equations (5) and (7) contain momentum flux uv and mass flux Cv, respectively. If the wall-normal velocity v = 0, equations (5) and (7) reduce to the conventional equations.

[15] On the basis of equation (5), *Yang* [2002] claimed that the log law is valid only when the wall-normal velocity is zero. As the wall-normal velocity is not zero in nonuniform, boundary layer flows [*Song and Chiew*, 2001; *Coles*, 1956], he concluded that the nonzero wall-normal velocity results in a deviation of measured streamwise velocity from the log law. This is why the wake function proposed by *Coles* [1956] is needed to express the velocity deviation. Similarly, for sediment-laden channel flow, it is necessary to investigate whether the wall-normal velocity v or the influence of momentum flux (uv) and mass flux (Cv) is negligible.

3. Influence of Wall-Normal Velocity v on Turbulent Structure and Sediment Concentration

[16] Strictly speaking, all open channel flows, regardless of the channel's geometry, are three dimensional, and $v \neq 0$ because of the presence of secondary currents [*Wang and Cheng*, 2005; *Yang et al.*, 2004b]. The addition of sediment particles to a clear water flow could alter the direction and magnitude of secondary currents in open channels, and subsequently the modification of secondary currents may result in velocity profiles in sediment-laden flows that differ from those in clear water. Though a theoretical relationship between secondary currents and sand particle motion is not available in the literature, researchers have already attributed some observed phenomena of sediment transport to secondary currents. For example, *Vanoni* [1946] observed that the spanwise distribution of sediment concentration varied periodically in rivers and open channels and inferred that this phenomenon might either generate or be generated by the secondary currents. Vanoni's observation was confirmed by *Kinoshita* [1967] using an aerial stereoscopic photosurvey of rivers in flood. His photos clearly showed that the low-speed zones were always associated with high sediment concentration. Kinoshita's observations are in agreement with *Immamoto and Ishigaki*'s [1988] and *Nezu*'s [2002] measurements (Figure 1). The flow speed is slower near the sidewall because of the sidewall effect, and the secondary currents transfer sediment from the bed to the surface. As a result, the sediment concentration at the surface near the sidewall is higher than that at the midchannel where the velocity is highest. In other words, these observations are in accordance with equations (7) and (8), which indicates that the upward (or positive) v results in the decrease of concentration gradient dC/dy. Furthermore, if $v = \omega$, equation (7) states dC/dy = 0 or the sediment concentration on the free surface is same as that in the bottom; hence the wall normal velocity conveys sediment from the bottom to the free surface, or the high-sediment-concentration zone on a river surface is always associated with upward secondary current, and vice versa. Thus it becomes understandable why *Vanoni* [1946] linked the periodically spanwise distribution of high sediment concentration on surface with the secondary currents.

[17] Many geologists and hydraulic engineers also noticed the existence of secondary currents in straight wide rivers (*Vanoni* [1946], *Nezu and Nakagawa* [1993], etc.). *Wang and Cheng*'s [2005] experiments clearly demonstrated that cellular secondary currents in a wide channel can be generated by uneven bed roughness as shown in Figure 1b. It is interesting to note the relationship between the secondary currents (Figure 1b) and Reynolds shear stress (Figure 1c) along profiles 1–1, 2–2 and 3–3 of Figure 1b. The data points along profiles 1–1 and 3–3 are systematically lower or higher than the expected values, i.e., $-\overline{u'v'}/u_*^2 = 1 - y/h$ which can only represent the measured values in profile 2–2.

[18] It can be seen from Figure 1b that in 1–1, the secondary current is downward (or $v < 0$); in 2–2, the secondary current is parallel to the free surface (or $v \approx 0$) and in 3–3 the secondary current is upward (or $v > 0$). Therefore the term uv/u_*^2 is negative, zero and positive in the profiles of 1–1, 2–2 and 3–3, respectively. This is why the measured Reynolds shear stresses in 1–1, 2–2 and 3–3 are lower, equal and higher than the predicted value. From equation (5) one may conclude that the alteration of direction of wall-normal velocity results in the deviation of Reynolds shear stress from standard linear distribution. In other words, equation (5) is consistent with the measured variation of data points shown in Figure 1c, suggesting that the difference between the data points and the dashed line may be represented by uv/u_*^2, in which case the wall-normal velocity v can be implicitly determined from the defect of Reynolds shear stresses. Since equation (5) can be rewritten as $(\overline{u'v'} - uv)/u_*^2 = 1 - y/h$, this alternative form indicates that the total shear stress, i.e., $(\overline{u'v'} - uv)/u_*^2$ remains

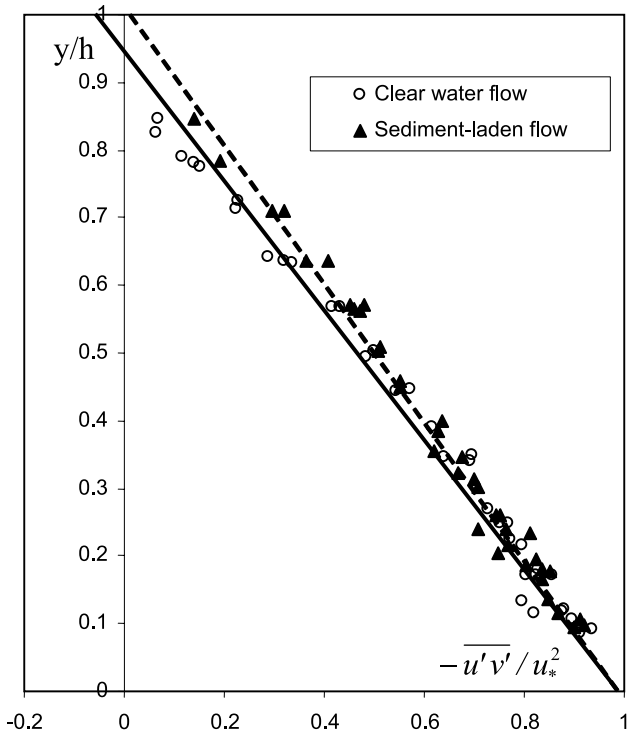

Figure 2. Reynolds shear stress distribution with or without sediment in a wide open channel (b/h = 7.0), measured by *Muste and Patel* [1997]; in the upper layer a discernible difference in Reynolds shear stress exists between clear water and sediment-laden flows.

unchanged as in 1-D flows and that uv can be regarded as a shear stress similar to the Reynolds shear stress. Hence it is understandable that uv can significantly affect the distribution of Reynolds shear stress [*Yang et al.*, 2004a].

[19] Next, it is worthwhile to investigate how sediment particles affect the wall-normal velocity. Equation (5) indicates that the nonzero wall-normal velocity will modify the Reynolds shear stress distribution. Thus, if the presence of sediment particles alters the velocity distribution, then certainly the Reynolds shear stress will be affected, i.e., the Reynolds shear stress in sediment-laden flows should differ from that in clear water flows.

[20] *Muste and Patel* [1997] measured the Reynolds shear stress distribution using DLDV system in a channel flow with and without sediment. In their measurements, the discharge, water depth, temperature and aspect ratio (b/h = 7) were held constant. The energy slope was slightly affected by the presence of sediment but the difference was less than 1.6%. The suspended concentration was increased steadily but no sediment deposited anywhere in the flume. The measured Reynolds shear stress is replotted in Figure 2, in which the shear velocity u_* was determined by extrapolation of measured Reynolds shear stress to the wall. In Figure 2 the dashed line represents the standard linear distribution, i.e., $1 - y/h$. The solid line best fits the data points from clear water flows. It is clear that the measured Reynolds shear stress of clear water flow deviates from the standard distribution, i.e., $1 - y/h$, this implies the existence of secondary currents.

[21] It is interesting to note that in Figure 2 the measured Reynolds shear stress in sediment-laden flows is systematically higher than that of clear water flows. This shift cannot be simply ascribed to measurement error but must be due to the presence of sediment because a similar shift is observed by *Cellino and Graf* [1999] (Figure 3), where the shear velocity was also determined by extrapolating the measured Reynolds shear stress to the wall.

[22] It can be seen from Figure 1a that in the centerline of upper layer, v is negative (downward); thus the term of uv/u_*^2 in equation (5) is negative in the upper layer. Near the free surface ($y/h \rightarrow 1$), equation (5) shows that $-\overline{u'v'}/u_*^2 \approx uv/u_*^2$. This is why the predicted Reynolds shear stress (see Figures 2 and 3) in the upper layer of clear water flow must be negative. Equation (5) also states that the zero shear stress occurs at the location of $y_m/h = 1 + uv/u_*^2$; thus it can be inferred that if zero Reynolds shear stress appears below the free surface ($y_m/h < 1$) as shown in Figures 2 and 3, the secondary current must be downward (or $v < 0$). Since the zero Reynolds shear always corresponds to the zero velocity gradient or the maximum velocity, it means that the maximum velocity u must appear below the free surface, i.e., the dip phenomenon occurs (see Figure 1a). Thus we can infer the existence of secondary currents on the basis of the distribution of Reynolds shear stress or the location of zero Reynolds shear stress. This inference is verified by *Muste and Patel* [1997, p. 744] as they observed that "weak secondary currents were undoubtedly present in the experiments in spite of the large aspect ratios employed. This was inferred from three distinct sand strips in the near-bed

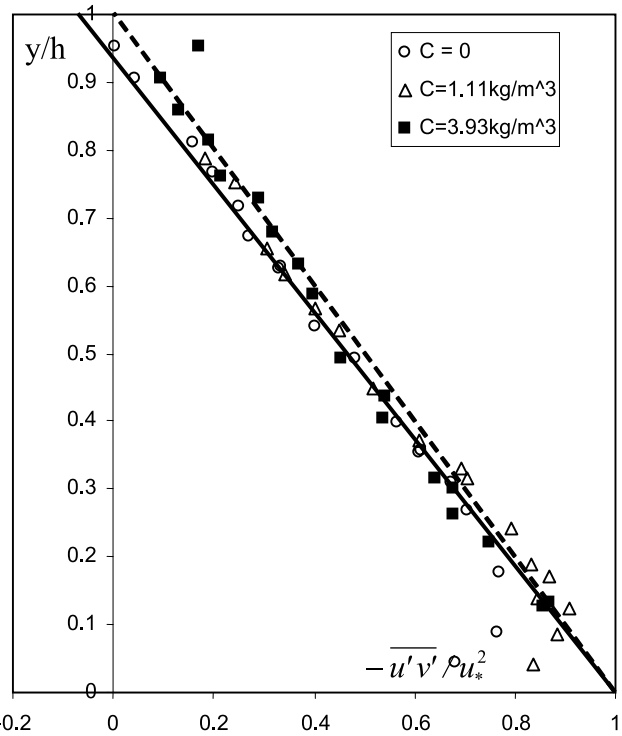

Figure 3. Reynolds shear stress distribution with or without sediment in an open channel (b/h = 5.0), as measured by *Cellino and Graf* [1999]; in the upper layer a discernible difference in Reynolds shear stress exists between clear water and sediment-laden flows.

region. As the concentration was increased, the number and widths of strips increased, coalescing at higher concentrations into a continuous layer of sand moving along the bed."

[23] From Figures 2 and 3 one may find that sediment particles indeed modify the Reynolds shear stress distribution, while from equation (5) one can infer that the Reynolds shear stress distribution could be affected by the momentum flux uv, or the variation of Reynolds shear stress between clear water and sediment-laden flows can be probably attributed to the nonzero wall-normal velocity. In other words, as Figures 2 and 3 show, the Reynolds shear stress increases after sediment particles are added to the clear water. This means that the magnitude of downward velocity v is reduced, or the presence of sediment induces an upward velocity that compensates the downward v caused by secondary currents. Hence the wall-normal velocity v can be written as follows:

$$\mathrm{v} = \mathrm{v}_1 + \mathrm{v}_2 \tag{9}$$

in which v_1 is the vertical velocity of clear water flow, which could be caused by secondary currents/nonuniformity and v_2 is the upward velocity induced by the presence of sediment particles.

[24] *Chien and Wan* [1999, p. 85] analyzed sediment settlement in river flows and concluded that sediment particles induce an upward fluid velocity which can be expressed as follows:

$$\mathrm{v}_2 = \frac{\mathrm{C}\omega}{1-\mathrm{C}} \tag{10}$$

Substitution of equation (9) into equation (5) yields

$$-\frac{\overline{\mathrm{u}'\mathrm{v}'}}{\mathrm{u}_*^2} = \left(1-\frac{\mathrm{y}}{\mathrm{h}}\right) + \frac{\mathrm{uv}_1}{\mathrm{u}_*^2} + \frac{\mathrm{uv}_2}{\mathrm{u}_*^2} \tag{11}$$

For clear water flows, *Yang et al.* [2004a] found that $\mathrm{uv}_1/\mathrm{u}_*^2$ approximately follows a linear relationship, i.e.,

$$\frac{\mathrm{uv}_1}{\mathrm{u}_*^2} = \alpha\frac{\mathrm{y}}{\mathrm{h}} \tag{12}$$

in which α = coefficient. Equation (12) indicates that α is caused by the nonzero wall-normal velocity v_1 that can be generated by secondary currents if the aspect ratio is small, or nonuniformity of flow. α in uniform and nonuniform flows can be determined using *Yang et al.*'s [2004a, 2006] empirical equations based on aspect ratio b/h and dh/dx.

[25] The eddy viscosity in equation (6) is often modeled by the following equation:

$$\varepsilon_f = lu_*\left(1-\frac{y}{h}\right) \tag{13}$$

where l is mixing length, equal to κy. Equation (13) is a modified form of Prandtl's mixing length theorem [*Bennett*, 1995]. *Yalin* [1977], *Wright and Parker* [2004a, 2004b] used equation (13) to describe the velocity profile in sediment-laden flows. Other researchers used it to derive the streamwise velocity profile in wave current flows [*You*, 1996, 1997] and in meandering and curved open channels [*Odgaard*, 1986; *Kikkawa et al.*, 1976]. *Cellino and Graf*'s [1999] experiments indicated that equation (11) can be approximately used to express the Reynolds shear stress in sediment-laden flows.

[26] The sediment diffusion coefficient is usually assumed to be identical or proportional to the fluid eddy viscosity, i.e.,

$$\varepsilon_s = \beta\varepsilon_f \tag{14}$$

where β is an empirical coefficient.

[27] The fall velocity ω in equation (10) can be assessed using a simple exponential relationship developed by *Richardson and Zaki* [1954],

$$\frac{\omega}{\omega_o} = (1-C)^{4.65} \tag{15}$$

where ω_o is the fall velocity of single particle that can be determined using Rubey's formula [*Chien and Wan*, 1999],

$$\omega_o = -6\frac{\nu}{d_{50}} + \sqrt{\left(6\frac{\nu}{d_{50}}\right)^2 + \frac{2}{3}\left(\frac{\rho_s}{\rho}-1\right)gd_{50}} \tag{16}$$

where ν is kinematic viscosity of fluid and d_{50} is median particle size.

[28] The governing equation for sediment concentration distribution can be obtained from equations (7), (8), (9), (10), (12), (13), and (14) with the following form:

$$\frac{dC}{d\xi} = -\frac{\omega}{\kappa\beta u_*}\frac{C}{\xi(1-\xi)} + \frac{C}{\beta\kappa\xi(1-\xi)u^+}\left(\alpha\xi + \frac{u^+\omega}{u_*}\frac{C}{1-C}\right) \tag{17}$$

where $\mathrm{u}^+ = \mathrm{u}/\mathrm{u}_*$ and $\xi = \mathrm{y}/\mathrm{h}$.

[29] Similarly, by inserting equations (6), (10), (12), and (13) into equation (11), one obtains the momentum equation for sediment-laden flows, i.e.,

$$\frac{du^+}{d\xi} = \frac{1}{\kappa\xi} - \frac{\alpha}{\kappa}\frac{1}{1-\xi} + \frac{u^+\omega}{\kappa u_*\xi(1-\xi)}\frac{C}{1-C} \tag{18}$$

It can be seen from equation (18) that for clear water flow, where C = 0 and $\kappa = \kappa_\mathrm{o}$ = clear water Karman constant, the integration of equation (18) yields

$$\frac{u}{u_*} = \left(\frac{u}{u_*}\right)_a + \frac{1}{\kappa_o}\ln\frac{\xi}{\xi_a} - \frac{\alpha}{\kappa_o}\ln(1-\xi) \tag{19}$$

where $(\mathrm{u}/\mathrm{u}_*)_\mathrm{a}$ is a nondimensional velocity at reference level ξ_a [*Wright and Parker*, 2004a], which is determined from measured data. For a channel flow without secondary currents, $\alpha = 0$ and equation (19) reduces to the classical log law.

[30] If the second term on the right-hand side of equation (17) is negligible, then the integration of equation (17) yields the Rouse law

$$\frac{C}{C_a} = \left(\frac{1-\xi}{\xi}\frac{\xi_a}{1-\xi_a}\right)^Z \tag{20}$$

where Z is Rouse number, equal to $\omega/(\kappa\beta u_*)$, and C_a is reference concentration at ξ_a.

[31] It is obvious that one can determine the velocity and sediment concentration distributions by solving the two first-order linear differential equations, i.e., equations (17) and (18) if the mixing length l or Karman constant is given.

4. Mixing Length in Neutrally Buoyant Sediment-Laden Flows ($\omega = 0$)

[32] To assess the variation of Karman constant κ, neutrally buoyant flow is investigated first. In this case, the last term on the RHS of equation (18) can be neglected because of $\omega = 0$. The mixing length theory developed by Prandtl postulates that in an analogy with the molecular motion of a gas, when a small fluid element moves in a flow field, its momentum does not change until the fluid element has moved a distance termed as the mixing length. Physically, it refers to the average path that fluid element can move freely without collision and momentum exchange. In the sediment-laden flows, the mixing length of fluid-sand mixture could be similar to that in clear water flows as the former can be physically treated as a homogeneous fluid whose density differs from that of clear water. Hence the mixing length of fluid-particle mixture has the following form:

$$l_m = \kappa_o y \tag{21}$$

As equation (13) is valid only for liquid phase, the mixing length l in equation (13) refers to the distance over which the liquid element changes its momentum. Since over the total length l_m, some of the space is occupied by solid particles, the averaged free path that water element remains its momentum unchanged should be reduced to

$$l = l_m(1 - \alpha_1\lambda) \tag{22}$$

in which α_1 is a factor and λ is the length occupied by solid particles or the linear concentration which is first introduced by *Elata and Ippen* [1961].

[33] It can be seen that for hyperconcentrated sediment-laden flow, the mixing length of liquid phase l or the free paths of water body is greatly suppressed by the solid particles; thus the turbulent fluctuations are significantly weakened. Therefore equation (22) provides an explanation why turbulence disappears in a hyperconcentrated flow as observed by *Chien and Wan* [1999, p. 535], who reported "...in northwest China where hyper-concentrated flows sometimes occur, the water surface is smooth, no ripples occur. Although distorted and deformed along their course, cloud-like patterns on the water surface maintain their identity over a rather long distance; clearly they do not mix in the usual way...."

[34] Consider a fluid-sediment mixture in which the volumetric concentration of the uniform spherical particles with diameter D is C. Assume the sediment particles are packed in a tetrahedral-rectangular fashion in such a way that the distance between the centers of the spheres becomes b_1D. The volume concentration C, i.e., the ratio between the space occupied by sediment particles, C_m to the whole space will be C_m/b_1^3. The free distance between the particles is $(b_1 - 1)D$. Hence $\lambda = D/[(b_1 - 1)D] = 1/(b_1 - 1)$, and $C = C_m/\{(1/\lambda) + 1)^3\}$. Thus the linear concentration is expressed as

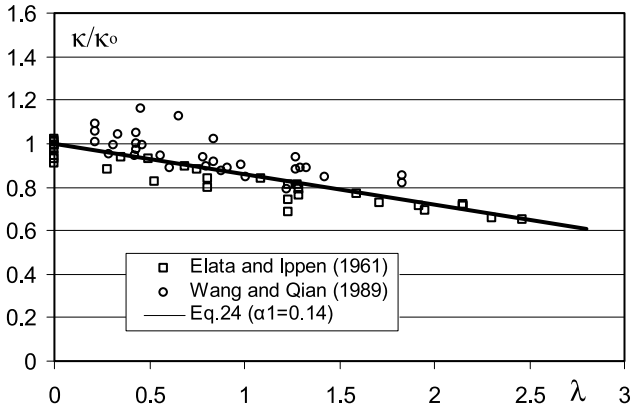

Figure 4. Comparison of the variation of the normalized Karman coefficient κ/κ_0 as a function of linear concentration λ measured by *Elata and Ippen* [1961] and *Wang and Qian* [1989] with equation (24) for $\alpha = 0.14$.

$$\lambda = \frac{1}{(C_m/C)^{1/3} - 1} \tag{23}$$

The maximum concentration $C_m = 0.74$.

[35] Equation (22) indicates that in sediment-laden flows, the liquid-phase mixing length l (= κy) is less than the total mixing length l_m. This conclusion is similar to that obtained by *Kovacs* [1998], who concluded that the presence of a solid phase in the sediment-laden flow reduces its free path of liquid phase or the mixing length.

[36] Equation (22) can be expressed equivalently in the following form:

$$\frac{\kappa}{\kappa_o} = 1 - \alpha_1\lambda \tag{24}$$

where κ is the Karman constant for sediment-laden flows.

[37] The experimental data sets of *Elata and Ippen* [1961] and *Wang and Qian* [1989] are used to test the validity of equation (24). Elata and Ippen's experiments were to identify the effect of density gradient of sediment on flows. They used plastic spheres with a specific gravity of 1.05; the spherical diameter varies within the range of 0.1 to 0.155 mm and the fall velocity is about 1 mm/s. The experiments were carried out in a 26.7 cm wide and 28.1 cm deep flume. During the experiments, high velocity was maintained to avoid sediment deposition. Similar experiments were conducted by *Wang and Qian* [1989]. The specific gravity of plastic particles was similar to that used by *Elata and Ippen* [1961]. The width of the smooth channel was 30 cm, and bed slope was 0.01. The maximum particle concentration was up to 20% by volume, and salt water was used so that the particles were neutrally buoyant.

[38] Figure 4 shows the plot of relative Karman coefficient as a function of the linear concentration, λ. It can be seen that the measured Karman coefficient decreases linearly as sediment concentration increases. The least squares method is used to determine the coefficient α_1 which is

Table 1. Summary of Flow and Sediment Conditions Given by *Einstein and Chien* [1955]

Run	Sand	d_{50}, mm	Q, L/s $\times 10^3$	B/h	u_*	$(u/u_*)_{\varepsilon=0.05}$	$C_{\varepsilon=0.05}(l/l)$	$C_{max}(g/l)$	α	β
C-1	coarse	1.3	78.2	2.14	11.92	9.59	0	0	0.65	
S-1	coarse	1.3	77.8	2.19	11.42	10.33	0.015	58	1	1
C-2	coarse	1.3	79.2	2.17	11.52	10.12	0	0	0.9	
C-3	coarse	1.3	73.3	2.44	13.73	10.87	0	0	−1.45	
S-2	coarse	1.3	73.9	2.50	12.85	11.83	0.058	121	1.6	1.25
S-3	coarse	1.3	73.3	2.59	13.27	11.24	0.064	151	2.5	1.43
S-4	coarse	1.3	73	2.61	14.23	14.25	0.082	198	2.4	1.67
S-5	coarse	1.3	73.3	2.70	14.53	11.32	0.11	328	3.5	2.13
C-4	coarse	1.3	73.3	2.48	12.60	13.53	0	0	0.2	
C-5	coarse	1.3	73.3	1.69	7.49	14.13	0	0	1.0	
C-6	medium	0.94	84	2.01	12.36	12.14	0	0	1.0	
S-6	medium	0.94	82	2.10	11.82	11.63	0.007	28	1	1
S-8	medium	0.94	79.8	2.16	11.64	12.67	0.016	112	1	1
S-9	medium	0.94	80.6	2.21	11.79	11.98	0.035	173	1.6	1
S-10	medium	0.94	79.8	2.27	12.68	11.58	0.054	263	1	1
C-7	medium	0.94	79.2	2.19	11.44	11.51	0	0	0.00	
C-8	medium	0.94	74.7	2.46	13.37	11.51	0	0	0.00	
C-9	medium	0.94	73.3	2.48	12.96	11.51	0	0	0.00	
C-10	fine	0.274	77.5	2.26	10.38	12.88	0	0	0.60	
C-11	fine	0.274	77	2.24	10.44	13.38	0	0	0.60	
S-11	fine	0.274	77.5	2.26	10.58	12.75	0.008	31	0.2	1
S-12	fine	0.274	77.2	2.27	10.05	11.81	0.042	205	1	1
C-12	fine	0.274	76.7	2.27	10.62	11.59	0	0	0.65	
S-13	fine	0.274	76.3	2.26	10.58	12.35	0.060	252	1.6	1
S-14	fine	0.274	76.3	2.42	12.05	12.54	0.088	386	1.8	1
S-15	fine	0.274	76.3	2.42	11.93	12.16	0.128	625	2.2	1

equal to 0.14. The linear relationship shown in Figure 4 indicates that in Prandtl's mixing length theorem, the movement of liquid phase or "liquid eddy" can be treated as a single air molecule that retains its momentum between the averaged free paths of air molecule. With the presence of sediment, the mixing length or "free path" of liquid phase is reduced for some space is occupied by solid particles; subsequently the Karman constant is reduced.

5. Velocity and Sediment Concentration Distributions in Buoyant Sediment-Laden Flows

5.1. Clear Water Flows

[39] In this study, reliable experiments carried out by *Einstein and Chien* [1955] are used to verify the proposed model because the data sets have been widely cited in the literature including textbooks (*Graf* [1971], *Chien and Wan* [1999], and *Yalin* [1977], etc.). The experiments were conducted in a 30-cm-wide channel. Characteristics of the flow and natural sediments are summarized in Table 1. The mean size of sediment was 1.3 mm for S-1 to S-5; 0.94 mm for S-6 to S-10; and 0.274 mm for S-11 to S-15. The hydraulic and sediment parameters like velocity profile and sediment concentration profiles were comprehensively measured. The Rouse number Z ranged from 0.8 to 3.2 covering the suspended and bed load dominant stages. The aspect ratios were rather small, in the range of 2 to 2.7. This clearly indicates that the flow was 3-D and secondary currents might exist. Clear water flows and sediment-laden flows were measured and compared, the energy slope and friction factor were kept relatively constant and sediment concentrations reached high values in some runs (up to 625 kg/m^3), indicating that large density gradients were present. Therefore this is a comprehensive and ideal data set to verify the proposed model because of the coexistence of secondary currents and high density gradient that might jointly generate the wall-normal velocity.

[40] In order to confirm the existence of nonzero wall-normal velocity, the measured velocity profiles in clear water flows are analyzed first and the results are presented in Figure 5. It can be seen clearly from Figure 5 that all measured velocity profiles except runs C-7, C-8 and C-9 cannot be represented by the classical log law, but equation (19) expresses the measured profiles very well. The good agreement between the data points and equation (19) indicates that the presence of nonzero wall-normal velocity plays an important role in the experiments. The wide range of α (from −1.45 to 1) is suggestive of weakly nonuniform flow because in uniform flows the parameter α only depends on the aspect ratios [*Yang et al.*, 2004a]. In this data set, since b/h was almost constant (2.0 to 2.7), α should also be constant. On the other hand, it is not rare for researchers to conduct experiments in weekly nonuniform flow as it is very difficult to generate a uniform flow and to maintain it during long measurement period. The conclusion that *Einstein and Chien* [1955, p. 15] conducted their experiments in weakly nonuniform flows is not surprising because they reported that "as the experiments were conducted in supercritical flow. . .. The uniformity of flow cannot be maintained, as a result the flow was far from uniform in most cases in this study. . . . The full significance of this nonuniformity has not been studied quantitatively yet."

[41] The influence of nonuniformity on v can be assessed from the integration of continuity equation as follows:

$$\int_0^y \left(\frac{\partial u}{\partial x}+\frac{\partial v}{\partial y}+\frac{\partial w}{\partial z}\right)dy = 0 \tag{25}$$

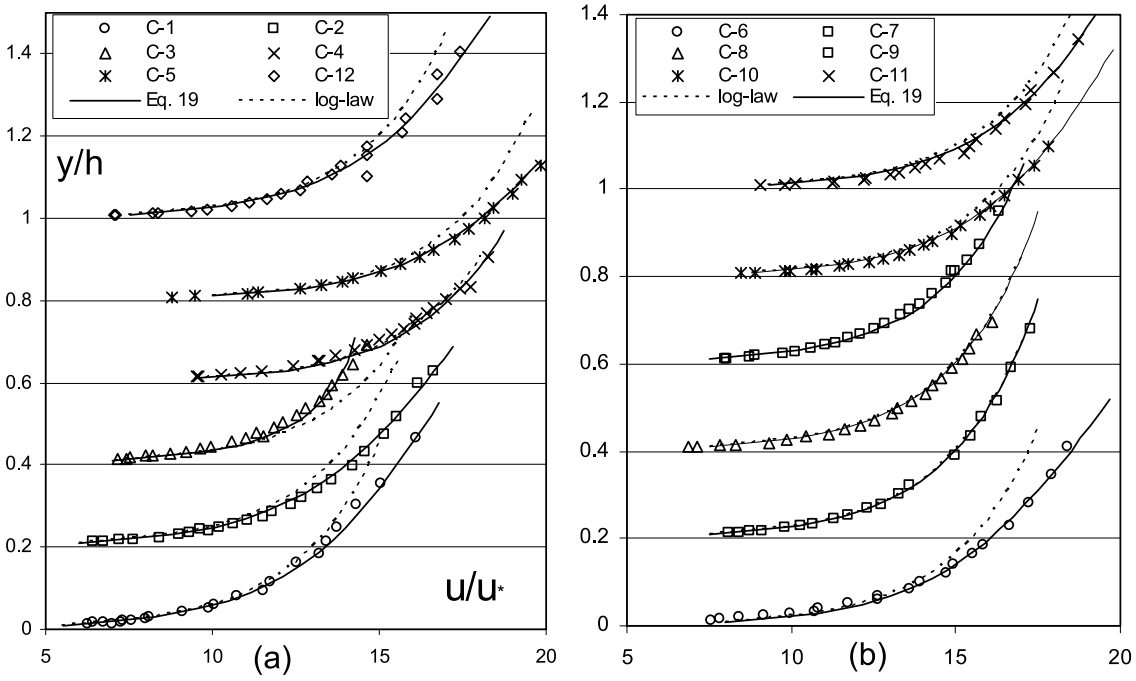

Figure 5. Comparison of measured velocity profiles in clear water flows by *Einstein and Chien* [1955] with classical log law (dotted lines) and equation (19) (solid lines); the deviations of data points from the log law indicate the existence of nonzero wall-normal velocity.

Along the symmetric centerline, $\partial w/\partial z = 0$; thus wall-normal velocity v can be determined from equation (25) as

$$v = -\int_0^y \frac{\partial u}{\partial x} dy \tag{26}$$

In a nonuniform flow, the acceleration $\partial u/\partial x$ could be either positive (accelerating flow) or negative (decelerating flow); thus the v could be upward or downward: This is why the coefficient α could be positive or negative (see equation (12)). *Yang et al.* [2006] analyzed the coefficient α in a nonuniform flow, and concluded that α can be theoretically determined if dh/dx, slope of channel bed, surface velocity, and aspect ratio are measured. Unfortunately, in this measurement, *Einstein and Chien* [1955] missed the nonuniform parameter, i.e., dh/dx.

[42] Figure 1a shows that the near-bed wall-normal velocity v is upward or positive, but equation (26) indicates that a downward or negative velocity v can be generated because of the nonuniformity; thus it can be inferred that under the joint action of secondary currents and nonuniformity, the resultant wall-normal velocity along the centerline in a nonuniform flow could be zero or negligible. In other words, the measured velocity profiles in nonuniform flows may still follow the classical log law. This conclusion is consistent with *Einstein and Chien*'s [1955] observations as shown in C-7, C-8 and C-9 of Figure 5. The good agreement between the measured velocity profiles and the log law does not mean no secondary currents in these experiments, but the secondary currents were deformed because of the nonuniformity, and the resultant wall-normal centerline velocity near the bottom is negligible.

[43] On the other hand, it can be inferred that the velocity would deviate from the log law in the outer flow region of runs C-7, C-8 and C-9 where the negative vertical velocity induced by nonuniformity was superimposed on the downward secondary currents (see Figure 1a), and the location of maximum velocity (velocity dip) should be lower than that in a uniform flow. *Einstein and Chien*'s [1955] experimental data of C-7, C-8 and C-9 does not support this conclusion because they only measured the velocity profile in the inner region (y/h < 0.4), no measurements were made in the outer flow region. However, *Kironoto and Graf* [1995] observed in their experiments that for the same aspect ratio (b/h = 2) the maximum velocity (velocity dip) occurred at y/h = 0.75 for a uniform-flow profile, but the velocity dip went down to y/h = 0.60 in an accelerating flow (negative v) and in the inner region the measured velocity profile follows the log law. Obviously, the present model's inference is in accordance with Kironoto and Graf's observation.

5.2. Sediment-Laden Flows

[44] This study uses the popular and most accurate fourth-order Runge-Kutta method to solve equations (17) and (18). The formulas used in the numerical solution are

$$\frac{dC}{d\xi} = f(\omega, \kappa, \xi, C, u^+) \tag{27}$$

$$\frac{du^+}{d\xi} = g(\omega, \kappa, \xi, C, u^+) \tag{28}$$

where f and g are functions expressed in equations (17) and (18).

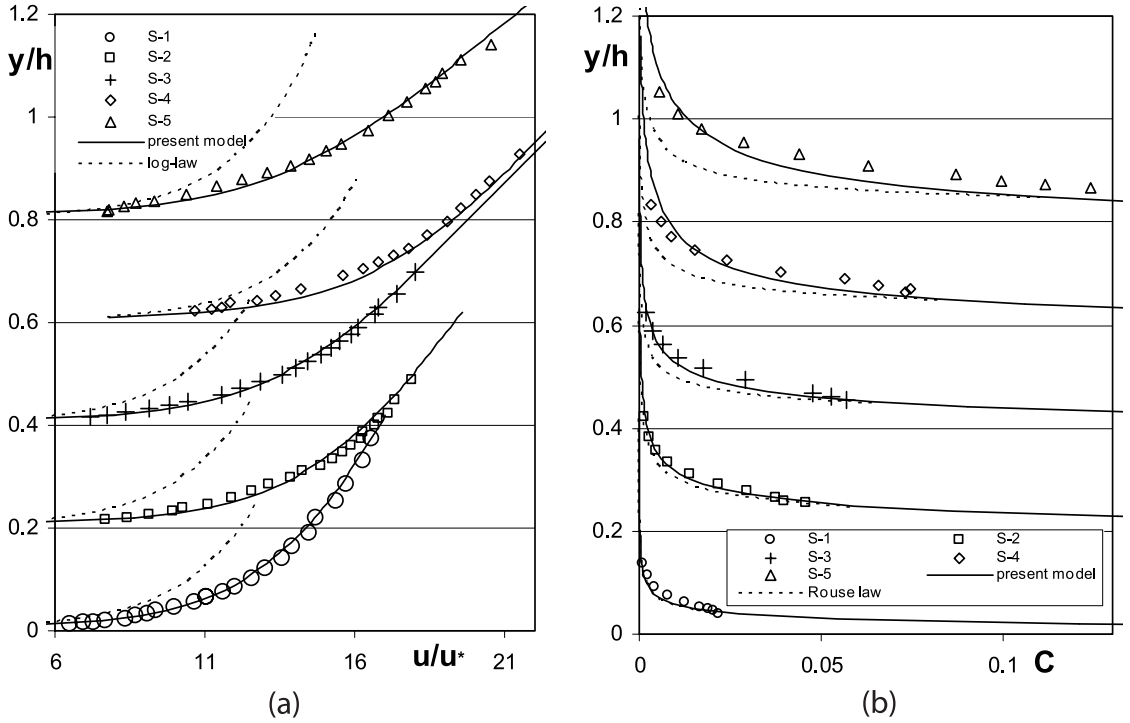

Figure 6. (a) Comparison of measured mean velocity profiles with the log law and present model and (b) comparison of measured sediment concentration with Rouse law and present model in coarse-sediment-laden (d_{50} = 1.3 mm) flows; data are from *Einstein and Chien* [1955].

[45] The unknown sediment concentration and velocity profiles are estimated as follows: (1) Determine the reference velocity (u^+_a) and sediment concentration (C_a) at the reference level (ξ_a) on the basis of measured velocity and sediment concentration. (2) Assume the values of parameter α and β (use α = 0 and β = 1 as a first estimate). (3) Calculate ω and κ using equations (15) and (24) based on C. (4) Calculate f and g on the basis of equations (17) and (18). (5) Estimate C and u^+ by solving equations (27) and (28) using the Runge-Kutta method [*Zill and Cullen*, 1992]. (6) Change parameter α and β and repeat steps 2–5 from $\xi = \xi_a$ to ξ = 1 until the calculated and measured profiles match each other.

[46] It is found that when the calculated and measured velocity profiles are in good agreement, all predicted sediment concentration can simultaneously match the measured concentration profiles. The results are presented in Figures 5–8, in which both log law and Rouse law are included. A slight difference is observed between the present model and Rouse law, or in other words the influence of wall-normal velocity on the concentration profile is less than that on the velocity profile.

[47] Figure 6a shows the predicted and measured velocity profiles of coarse sediment (S-1 to S-5). The comparison of sediment concentration is shown in Figure 6b. It can be seen that the agreement is very good. However, it is also found that the sediment diffusion coefficient in such cases is not the same as the turbulent eddy viscosity. That is, β in equation (14) is greater than 1 and increases with the increasing sediment concentration. This is consistent with *van Rijn* [1984] and *Nezu and Azuma*'s [2004] conclusions, the former found by analyzing measured data that for coarse sand, the parameter β should be greater than unity, and the latter experimentally found that the coefficient β increases with sediment concentration.

[48] Figures 7 and 8 show the predictions of medium and fine sediments, respectively. The good agreement between the measured and predicted sediment concentration profiles demonstrates that for medium and fine sediments, it is not necessary to correct the sediment diffusion coefficient (β = 1). It is also interesting to note that given appropriate values for α, equations (17) and (18) yield simultaneously good agreements with the measured velocity and sediment concentration. Equations (17) and (18) state that the deviations of measured velocity from the log law and sediment concentration from the Rouse law are caused by the wall-normal velocity, the slight difference between Rouse law and the present model shown in Figures 7b and 8b indicates that the concentration profiles are insensitive to the wall-normal velocity relative to the velocity profiles. This is probably why so many researchers discover that the log law is invalid in sediment-laden flows, while few investigators report the invalidity of Rouse law in literature.

[49] From Table 1 one can seen that $\alpha = \beta = 1$ is obtained for runs S-1, S-6, S-8, S-10 and S-12 in which the sediment concentration ranges from 28 kg/m^3 to 263 kg/m^3. This implies that α is independent of sediment concentration. The velocity or concentration difference in these runs is caused by the density stratification or the wall-normal velocity induced by sediment settling.

[50] The data and model indicate that wall-normal velocities can be induced by the characteristics of the flow (secondary currents or nonuniformity) and sediment settling (or Richardson number). Anyone who wants to assess the

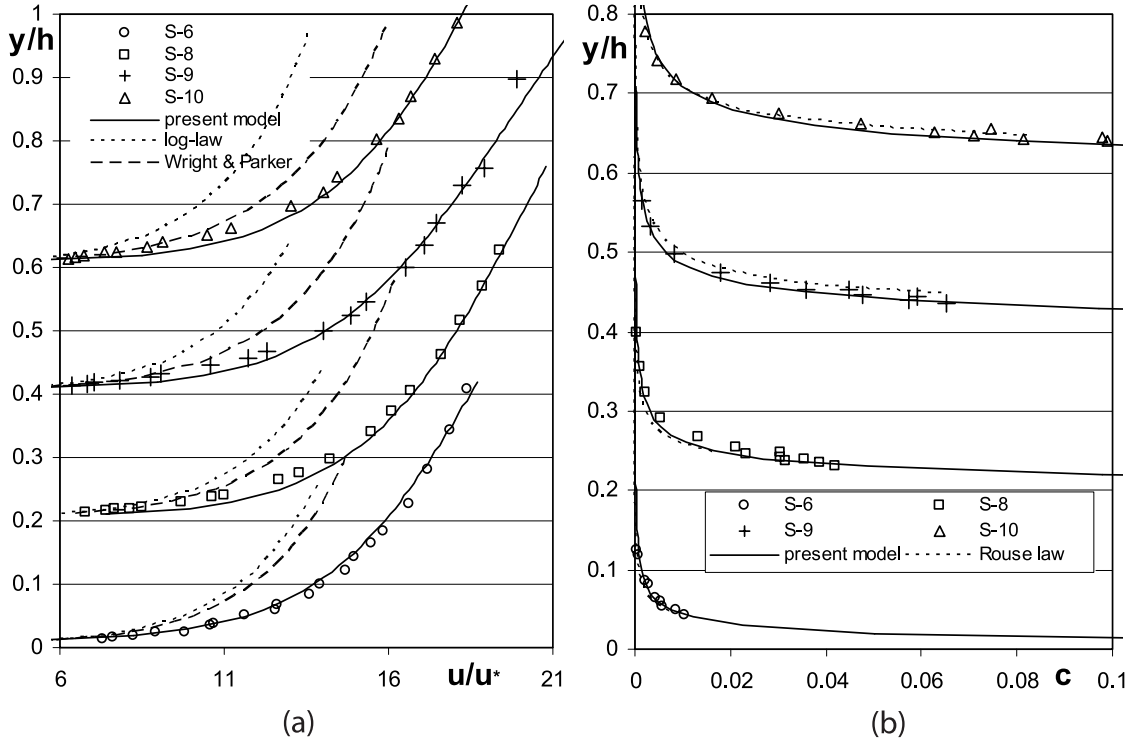

Figure 7. (a) Comparison of measured mean velocity profiles with log law, present model, and *Wright and Parker*'s [2004b] model and (b) comparison of measured sediment concentration with Rouse law and present model in medium-sediment-laden (d_{50} = 0.94 mm) flows; data are from *Einstein and Chien* [1955].

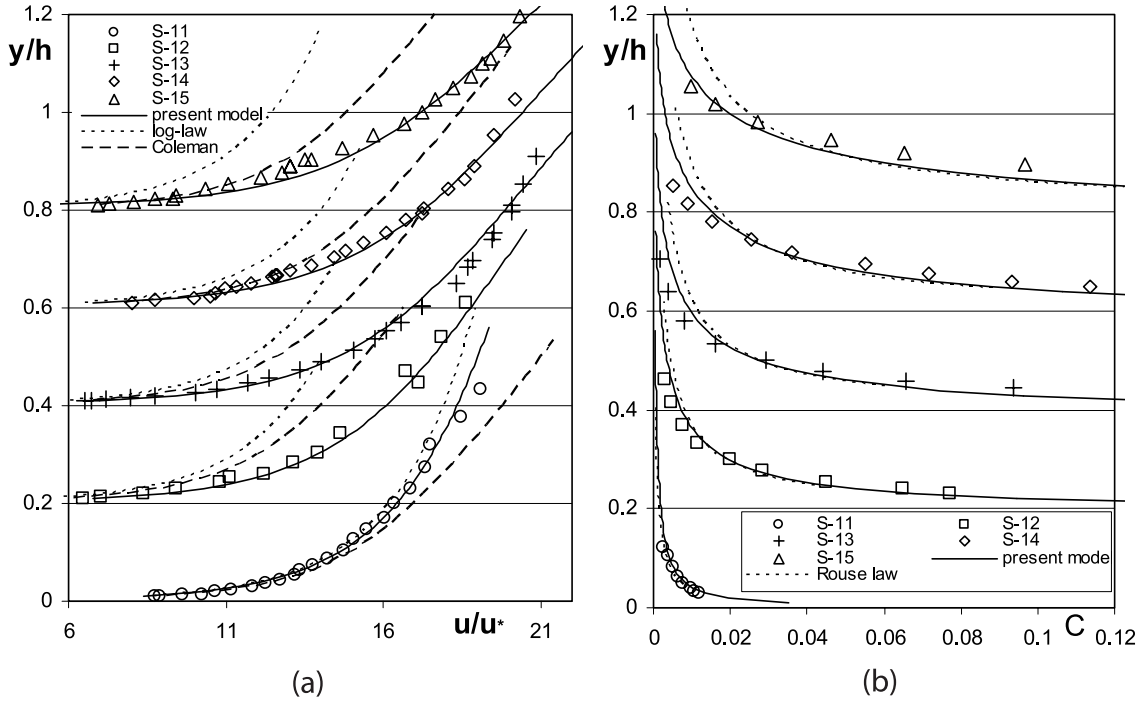

Figure 8. (a) Comparison of measured mean velocity profiles with log law, present model, and *Coleman*'s [1981] model and (b) comparison of measured sediment concentration with Rouse law and present model in fine-sediment-laden (d_{50} = 0.274 mm) flows; data are from *Einstein and Chien* [1955].

influence of sediment on velocity profile should eliminate the effect of secondary currents; otherwise the influence of the characteristics of the flow would be wrongly treated as the influence of sediment.

[51] Wall-normal velocities caused by the characteristics of the flow are negligible only in the near-bed region but can be significant in the upper layer (equation (12)). Conversely, sediment settling has a larger effect near the bed relative to the upper layer (equation (10)). Therefore it can be inferred that the upward velocity induced by sediment settling would attenuate the lower secondary current in Figure 1, but the upper cell of secondary current would be strengthened relative to the secondary currents in clear water flows. The model presented here can yield good results because these two factors are included.

6. Discussion

[52] As aforementioned, in the years since *Vanoni* [1946] and *Einstein and Chien* [1955] experimentally observed the reduction of the Karman coefficient in flows with presence of suspended sediment, many sophisticated models have been developed to express this phenomenon, such as log wake model by *Coleman* [1981] or by *Wang et al.* [2001], kinetic model by *Fu et al.* [2005], density stratification model by *Wright and Parker* [2004a, 2004b], etc. Most previous researchers hypothesized that the presence of suspended particles modify the turbulent structures, and they often related the turbulent eddy viscosity with Richardson number.

[53] However, like *Coleman*'s [1981] log wake model, this study assumes that the density gradient only affects the mean flow structure, not the turbulent structure. To clarify the difference between this and the previous models, it would be useful to compare various predictions with the measured data. Complete comparison between this model and numerical models is very difficult and beyond the scope of the study; thus only the simplified models proposed by *Wright and Parker* [2004b] and *Coleman* [1981] are discussed and compared.

[54] The density stratification model developed by *Wright and Parker* [2004a] is very complex; thus its simplified model [*Wright and Parker*, 2004b] is used for comparison, that is

$$\frac{u}{u_*} = \frac{u_a}{u_*} + \frac{1}{m\kappa_o} \ln\left(\frac{\xi}{\xi_a}\right) \tag{29}$$

where

$$m = \begin{cases} 1 - 0.06\left(\dfrac{C_{0.05}}{S}\right)^{0.77} & for \quad C_{0.05}/S \le 10 \\ 0.67 - 0.0025\dfrac{C_{0.05}}{S} & for \quad C_{0.05}/S > 10 \end{cases} \tag{30}$$

in which $C_{0.05}$ is the concentration by volume at y = 0.05h and S is the energy slope.

[55] *Coleman*'s [1981] model can be simplified as follows:

$$\frac{u}{u_*} = \frac{u_a}{u_*} + \frac{1}{\kappa_o} \ln\frac{\xi}{\xi_a} + \frac{2\Pi}{\kappa_o} \sin^2\left(\frac{\pi}{2}\ \xi\right) \tag{31}$$

where Π is the wake coefficient and is empirically expressed by

$$\Pi = 0.2\sqrt{1 + R_i} - 0.01R_i - 0.13 \tag{32a}$$

in which R_i is the Richardson number and defined as follows:

$$R_i = \frac{gh}{u_*^2} \frac{\rho_{0.05} - \rho_h}{\overline{\rho}} \tag{32b}$$

where $\overline{\rho}$ is the average density of suspension, ρ_h the density of suspension at y = h and $\rho_{0.05}$ the density at y = 0.05 h.

[56] *Wright and Parker*'s [2004b] simplified model is included in Figure 7a, and *Coleman*'s [1981] model is included in Figure 8a. It can be seen that both *Wright and Parker*'s [2004b] and *Coleman*'s [1981] models are better than the log law, but the agreements with experimental data are not very good. The poor agreement could be ascribed to the simplifying assumptions made in their models, which might be violated in *Einstein and Chien*'s [1955] data set because in clear water flows (C = 0) both *Wright and Parker*'s [2004a, 2004b] and *Coleman*'s [1981] models revert to the classical log law that is applicable only in uniform flows, but as shown in Figure 5, Einstein and Chien's data were collected from the nonuniform flows.

[57] *Wright and Parker*'s [2004a] model, like almost all existing models, attributes the velocity variation to density stratification which produces an upward buoyant force. They defined the Richardson number as follows:

$$R_i = \left(\frac{\rho_s}{\rho} - 1\right) g\ \frac{\omega C}{u_*^2(1-\xi)du/dy} \tag{33}$$

Comparing equation (33) with equation (10) and noticing $1 - C \approx 1$, one can find that ωC in the numerator of equation (33) is actually the upward velocity v_2 in equation (10); thus we can say that as the Richardson number represents the ratio of kinetic energy lost working against the settlement to the kinetic energy generated by shear, it is an index of upward velocity v_2 induced by sediment settlement. Equation (11) can be rewritten as follows by introducing the Richardson number R_i:

$$-\frac{\overline{u'v'}}{u_*^2(1-\xi)} = 1 + \frac{uv_1}{u_*^2(1-\xi)} + aR_i \tag{34}$$

where a is a factor independent of sediment concentration and $a = du^2/dy/[2(\rho_s/\rho - 1)g])$, and aR_i is less than 1.

[58] If the wall-normal velocity v_1 caused by secondary currents/nonuniformity is assumed to be negligible, then equation (34) can be written in the following form:

$$\frac{\varepsilon_f}{1 + aR_i}\frac{du}{dy} = \varepsilon_m \frac{du}{dy} = u_*^2(1-\xi) \tag{35a}$$

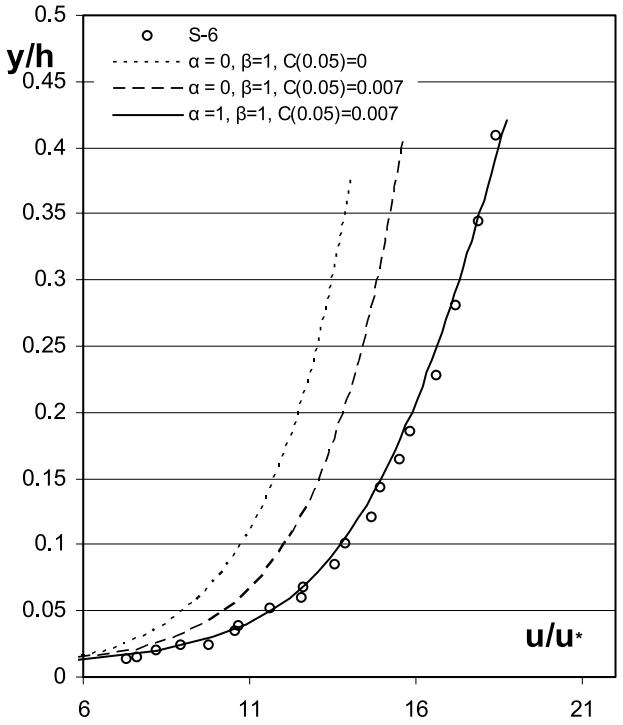

Figure 9. Influence of wall-normal velocity v_1 caused by flow noninformality ($\alpha \neq 0$) and v_2 caused by sediment settlement on streamwise velocity based on run S-6 of *Einstein and Chien* [1955], where C(0.05) denotes the concentration at $\xi = 0.05$.

where ε_m = eddy viscosity of sand-water mixture. If the Taylor series expansion is applied, the relationship between ε_m and ε_f can be expressed as follows:

$$\varepsilon_m = \frac{\varepsilon_f}{1 + aR_i} = \varepsilon_f \left[1 - aR_i + (aR_i)^2 - (aR_i)^3 + \cdots\right] \tag{35b}$$

if the first two terms in equation (35b) are kept, one obtains

$$\varepsilon_m = \varepsilon_f (1 - aR_i) \tag{35c}$$

Equation (35c) was developed by *Smith and McLean* [1977] and was applied by *Wright and Parker* [2004a]. Thus one can conclude that the present model is consistent with previous studies, and the effect of density stratification has been included in the model, or the present model reduces to Wright and Parker's model if $v_1 = 0$ is assumed. As *Einstein and Chien* [1955] conducted the measurement in nonuniform flows, and v_1 was nonzero, this is why Wright and Parker's simplified model cannot express the measured velocity well, as shown in Figure 7.

[59] Because the present model hypothesizes that the wall-normal velocity v caused by sediment settling and secondary currents jointly deviates the velocity from the log law, it would be useful to identify clearly the relative importance of these two causes. Figure 9 is plotted for this purpose, and S-6 is selected for the comparison. First, the parameters α and C are set to zero and $\beta = 1$, this means the second and third terms can be dropped from equation (18), after which the log law can be obtained by integrating equation (18). Second, $\alpha = 0$, $C_{\xi=0.05} = 0.07$ and $\beta = 1$ are used in the calculation of equation (18), this means that only the wall-normal velocity caused by sediment settling is considered. It can be seen from Figure 9 that higher velocity is obtained relative to the log law. This implies that sediment settlement can indeed increase the normalized velocity u/u_*. Third, by adjusting the parameter α, one can fit the measured data point with good agreement as shown in Figure 9, which indicates that the influence of secondary current due to small aspect ratio and nonuniformity on the streamwise velocity profile should not be underestimated.

[60] This study mainly discusses the laboratory flows, but the model can be easily extended to natural river flows. In this model, essentially there exists one unknown parameter α (in natural river flows $\beta = 1$ can be assumed because of low concentration); α can be determined from the velocity dip, which is the most important feature of secondary currents. Obviously, at the velocity dip, $du^+/d\xi = 0$, from equation (18), one has

$$\alpha = \frac{1 - \xi_m}{\xi_m} + u_m^+ \frac{C_m}{1 - C_m} \frac{\omega}{u_*} \approx \frac{1}{\xi_m} - 1 \tag{36}$$

where the subscript m denotes the position of maximum velocity. Hence the parameter α can be determined on the basis of the location of dip phenomenon, so that the model can be applied in natural rivers.

7. Conclusions

[61] A theoretical analysis of suspended sediment-laden flow in an open channel has been conducted. The good agreement between the proposed model and experimental data leads to the following conclusions:

[62] 1. For clear water flows, the wall-normal velocity could be induced by secondary currents or nonuniformity, which subsequently results in an additional momentum flux (uv) and leads to the velocity deviation from the classical log law. This additional momentum flux is larger in the upper layer relative to that in the bed region.

[63] 2. For sediment-laden flows, the magnitude of wall-normal velocity v could be influenced by the presence of sediment. The momentum flux uv and mass flux Cv jointly exert significant influence on the vertical profiles of horizontal velocity and sediment concentration.

[64] 3. For neutrally buoyant sediment flows, the reduction of Karman coefficient is the result of reduced free path of fluid particles; and the influence of sediment concentration on Karman coefficient still exists in buoyant sediment-laden flows.

[65] 4. The traditional momentum equation and sediment continuity equation neglect the terms of uv and Cv under assumption of v = 0, which results in the invalidity of log law and Rouse law for the velocity and concentration profiles when v is not zero. This study clearly demonstrates that uv and Cv should be included in these equations, in which case the velocity and concentration profiles can be well reproduced.

[66] 5. The study reveals that the nonzero wall-normal velocity driven by the density stratification plays a crucial

role for the velocity deviation from the log law. Such wall-normal velocity could be also caused by thermal stratification; this is why in meteorological boundary layer with temperature gradient, the velocity does not follow the log law.

Notation

a	factor.
b_1	distance between particles.
b	reference level from bed.
C	mean volumetric sediment concentration.
C'	sediment concentration fluctuation.
C_a	reference concentration.
C_m	maximum sediment concentration (for spherical particles $C_m = 0.74$).
D	particle diameter.
d_{50}	median sediment size.
g	gravitational acceleration.
h	water depth.
l	mixing length, equal to κy.
l_w	mixing length of fluid particles.
l_m	mixing length of liquid-solid mixture.
R_i	Richardson number.
S	energy slope.
u	streamwise velocity.
$u^+ = u/u_*$	
u_a	velocity at reference level ξ_a.
u_*	shear velocity, equal to $(gRS)^{0.5}$.
$(u/u_*)_a$	nondimensional velocity at reference level ξ_a.
uv and uw	momentum fluxes caused by mean velocities.
v	vertical velocity in y directions.
w	lateral velocity in z directions.
x	streamwise direction.
y	vertical direction.
y_o	the apparent bottom roughness (for smooth boundary $y_o = \nu/9u_*$, for roughened boundary, $y_o = \Delta/30$).
z	lateral direction.
Z	Rouse number, equal to $\omega/(\kappa u_*)$.
α	coefficient.
β	coefficient.
ε_f	eddy viscosity of liquid phase.
ε_s	sediment diffusion coefficient.
ε_m	eddy viscosity of water-sand mixture.
ξ	relative water depth, equal to y/h.
ξ_a	reference level.
κ_o	standard Karman constant, equal to 0.4.
κ	Karman constant for sediment-laden flows.
λ	linear concentration.
μ	dynamic viscosity.
ν	kinetic viscosity.
ρ_s	density of sediment.
ρ	water density.
$\overline{\rho}$	average density of suspension.
τ_{xy}	shear stress = $\mu du / dy - \rho\overline{u'v'}$.
τ_{xz}	shear stress = $\mu du / dz - \rho\overline{u'w'}$.
ω	fall velocity of sediment particles.
ω_o	fall velocity of a single sediment particle.
$-\rho\overline{u'w'}$, $-\rho\overline{u'v'}$	Reynolds shear stress.
Π	wake coefficient.

[67] **Acknowledgments.** The writer thanks the associate editor Patricia L. Wiberg and the reviewer S. Wright for their valuable comments and suggestions.

References

Bennett, J. P. (1995), Algorithm for resistance to flow and transport in sand-bed channels, *J. Hydraul. Eng.*, *121*(8), 578–590.

Bennett, S. J., J. S. Bridge, and J. L. Best (1998), Fluid and sediment dynamics of upper stage plane beds, *J. Geophys. Res.*, *103*, 1239–1274.

Best, J., S. Bennett, J. Bridge, and M. Leeder (1997), Turbulence modulation and paricle velocities over flat sand beds at low transport rates, *J. Hydraul. Eng.*, *123*(12), 1118–1129.

Cellino, M., and W. H. Graf (1999), Sediment-laden flow in open-channels under noncapacity and capacity conditions, *J. Hydraul. Eng.*, *125*(5), 455–462.

Chien, N., and Z. Wan (1999), *Mechanics of Sediment Transport*, Am. Soc. Civ. Eng., Reston, Va.

Cioffi, F., and F. Gallerano (1991), Velocity and concentration profiles of solid particles in a channel with movable and erodible bed, *J. Hydraul. Eng.*, *129*(3), 387–401.

Coleman, N. L. (1981), Velocity profile with suspended sediment, *J. Hydraul. Res.*, *19*(3), 211–229.

Coleman, N. L. (1986), Effects of suspended sediment on open-channel distribution, *Water Resour. Res.*, *22*(10), 1377–1384.

Coles, D. (1956), The law of the wake in the turbulent boundary layer, *J. Fluid Mech.*, *1*, 191–226.

Einstein, H. A., and N. Chien (1955), Effects of heavy sediment concentration near the bed on velocity and sediment distribution, *Rep. 8*, Mo. River Div., U.S. Army Corps of Eng., Omaha, Nebr.

Elata, C., and A. T. Ippen (1961), The dynamics of open channel flow with suspensions of neutrally buoyant particles, *Tech. Rep. 45*, Hydrodyn. Lab., Mass. Inst. of Technol., Cambridge.

Fu, X., G. Wang, and X. Shao (2005), Vertical dispersion of fine and coarse sediment in turbulent open channel flows, *J. Hydraul. Eng.*, *131*(10), 877–888.

Graf, E. H. (1971), *Hydraulics of Sediment Transport*, McGraw-Hill, New York.

Guo, J., and P. Y. Julien (2001), Turbulent velocity profiles in sediment-laden flows, *J. Hydraul. Res.*, *39*(1), 11–23.

Hawksley, P. G. W. (1951), The effect of concentration on the settling of suspensions and flow through porous media, in *Some Aspects of Fluid Flow*, pp. 114–135, Edward Arnold, London.

Immamoto, H., and T. Ishigaki (1988), Measurement of secondary flow in an open channel, paper presented at 6th IAHR-APD Congress, Int. Assoc. for Hydraul. Res., Kyoto, Japan.

Kikkawa, H., S. Ikeda, and A. Kitagawa (1976), Flow and bed topography in curved open channels, *J. Hydraul. Div. Am. Soc. Civ. Eng.*, *102*(2), 1327–1342.

Kinoshita, R. (1967), An analysis of the movement of flood waters by aerial photography: Concerning characteristics of turbulence and surface flow (in Japanese), *Photogr. Surv.*, *6*, 1–17.

Kironoto, B. A., and W. H. Graf (1995), Turbulence characteristics in rough non-uniform open-channel flow, *Proc. Inst. Civ. Eng. Water Marit. Energy*, *112*(12), 336–348.

Kovacs, A. E. (1998), Prandtl's mixing length concept modified for equilibrium sediment-laden flows, *J. Hydraul. Eng.*, *124*(8), 803–812.

Kreeselidze, N. B., and V. I. Kutavaia (1995), Experimental research on kinematics of flows with high suspended solid concentration, *J. Hydraul. Res.*, *33*(1), 65–75.

Lyn, D. A. (1988), A similarity approach to turbulent sediment-laden flows in open channels, *J. Fluid Mech.*, *193*, 1–26.

Muste, M., and V. C. Patel (1997), Velocity profiles for particles and liquid in open channel flow with suspended sediment, *J. Hydraul. Eng.*, *123*(9), 742–751.

Nezu, I. (2002), Open-channel turbulence and its research prospect in the new century, paper presented at 13th IAHR-APD Congress, Int. Assoc. for Hydraul. Res., Singapore.

Nezu, I., and R. Azuma (2004), Turbulence characteristics and interaction between particles and fluid in particle-laden open channel flows, *J. Hydraul. Eng.*, *130*(10), 988–1001.

Nezu, I., and H. Nakagawa (1993), *Turbulence in Open-Channel Flows*, A. A. Balkema, Brookfield, Vt.

Odgaard, A. J. (1986), Meander flow model I: Development, *J. Hydraul. Eng.*, *112*(12), 1117–1150.

Parker, G., and N. L. Coleman (1986), Simple model of sediment-laden flows, *J. Hydraul. Eng.*, *112*(5), 356–375.

Richardson, J. F., and W. N. Zaki (1954), Sedimentation and fluidization. part 1, *Trans. Inst. Chem. Eng.*, *32*(1), 35–53.
Smith, J. D., and S. R. McLean (1977), Spatially averaged flow over wavy surface, *J. Geophys. Res.*, *82*(12), 1735–1746.
Song, T., and Y. M. Chiew (2001), Turbulence measurement in nonuniform open-channel flow using acoustic Doppler velocimeter (ADV), *J. Eng. Mech.*, *127*(3), 219–232.
Steinour, H. H. (1944a), Rate of sedimentation: part 1. Nonflocculated suspensions of uniform spheres, *Ind. Eng. Chem.*, *36*(7), 618–624.
Steinour, H. H. (1944b), Rate of sedimentation: part 2. Suspensions of uniform size angular particles, *Ind. Eng. Chem.*, *36*(9), 840–847.
Steinour, H. H. (1944c), Rate of sedimentation: part 3. Concentrated flocculated suspensions of powders, *Ind. Eng. Chem.*, *36*(10), 901–907.
Vanoni, V. A. (1946), Transportation of suspended sediment by running water, *Trans. Am. Soc. Civ. Eng.*, *111*, 67–133.
Vanoni, V. A., and G. N. Nomicos (1960), Resistance properties in sediment-laden streams, *Trans. Am. Soc. Civ. Eng.*, *125*, 1140–1175.
van Rijn, L. C. (1984), Sediment transport, part II: Suspended load transport, *J. Hydraul. Eng.*, *110*(11), 1613–1641.
Wang, X. K., and N. Qian (1989), Turbulence characteristics of sediment-laden flow, *J. Hydraul. Eng.*, *115*(6), 781–800.
Wang, X. K., Z. Y. Wang, and D. X. Li (2001), Velocity profile of sediment suspensions and comparison of log-law and wake-law, *J. Hydraul. Res.*, *39*(2), 211–217.
Wang, Z. Q., and N. S. Cheng (2005), Secondary flows over artificial bed strips, *Adv. Water Resour.*, *28*(5), 441–450.
Wright, S., and G. Parker (2004a), Density stratification effects in sand-bed rivers, *J. Hydraul. Eng.*, *130*(8), 783–795.
Wright, S., and G. Parker (2004b), Flow resistance and suspended load in sand-bed rivers: Simplified stratification model, *J. Hydraul. Eng.*, *130*(8), 796–805.
Yalin, M. S. (1977), *Mechanics of Sediment Transport*, Elsevier, New York.
Yang, S.-Q. (2002), 1st and 2nd order approximate solutions of Reynolds equation in 3-D channel flows, paper presented at 13th APD-IAHR Congress, Int. Assoc. for Hydraul. Res., Singapore, 6–8 Aug.
Yang, S. Q., and A. J. McCorquodale (2004), Determination of boundary shear stress and Reynolds shear stress in smooth rectangular channel flows, *J. Hydraul. Eng.*, *130*(5), 458–462.
Yang, S. Q., S. K. Tan, and S. Y. Lim (2004a), Velocity distribution and dip-phenomenon in smooth uniform open channel flows, *J. Hydraul. Eng.*, *130*(12), 1179–1186.
Yang, S. Q., S. K. Tan, and S. Y. Lim (2004b), Velocity and sediment concentration profiles in sediment-laden flows, *China Ocean Eng.*, *18*(2), 229–244.
Yang, S. Q., W. L. Xu, and G. L. Yu (2006), Velocity distribution in a gradually accelerating flow, *Adv. Water Resour.*, *29*(12), 1969–1980.
You, Z. J. (1996), The effect of wave-induced stress on current profiles, *Ocean Eng.*, *23*, 619–628.
You, Z. J. (1997), On the vertical distribution of $\langle \tilde{u}\tilde{w} \rangle$: Discussion, *Ocean Eng.*, *30*, 305–310.
Zill, D. G., and M. R. Cullen (1992), *Advanced Engineering Mathematics*, PWS, Boston, Mass.

S.-Q. Yang, School of Environmental Science and Engineering, South China University of Technology, Wushan, Guangzhou, 510640, China. (csqyang@ntu.edu.sg)